Jestr

Journal of Engineering Science and Technology Review 15 (2) (2022) 91 - 101

JOURNAL OF
Engineering Science and Technology Review

Research Article

www.jestr.org

A Theoretical Study to Predict the Flexural Strength of Singly and Doubly Reinforced Ultra-High Performance Concrete Beams

Adil M. Jabbar[1,*], Qais A. Hasan[2] and Zinah A. Abdul-Husain[2]

[1]*Civil Engineering Department, College of Engineering, Wasit University, Iraq.*
[2]*Civil Engineering Department, University of Technology, Baghdad, Iraq.*

Received 9 March 2022; Accepted 29 April 2022

Abstract

Ultra-high performance concrete (UHPC) characterizes by a significant tensile strength that cannot be neglected in structural analysis, besides more than 150 MPa compressive strength, high ductility, durability, and toughness. The available analytical methods for traditional concrete beams disregard the tensile strength and strain-softening behavior in tension and compression; therefore, they are not suitable for analyzing UHPC beams. This paper presents a theoretical study to predict the flexural capacity of UHPC beams based on an analysis method that considers the effect of material properties. Predicting the bending moment in singly and doubly reinforced UHPC beams depends on adopting a simplified tensile and compressive constitutive response of UHPC.The procedure adopts several factors that affect the behavior of UHPC upon loading. Previous factors like volume fraction, shape, length, diameter, and orientation of fibers are considered for estimating the tensile stress and a bending moment of UHPC. In addition, a new factor related to silica fume content is adopted to estimate the bonding force between fibers and the matrix and the tensile stress. Also, the initial tensile strength of UHPC is deemed in the tensile stress equation due to the dual action of fibers on confining the matrix and the bridging effect by transferring the stress upon cracking. The equations are proposed for counting the tensile stress, neutral axis position of the beam section, and bending moment. These equations agree with the experimental results for tensile stress and a bending moment of beams implemented by other researchers.

Keywords: UHPC, steel fibers, compressive strength, tensile stress, flexural analysis

1. Introduction

Fiber-reinforced concrete (FRC) was introduced as the most effective method to overcome the brittleness and enhance the tensile strength [1, 2]. FRC enhances the stress-transfer capacity beyond concrete cracking by strain-softening behavior [3]. Fibers transfer the stress across the crack, between the two sides of the matrix; therefore, they improve the post-cracking tensile behavior and enhance the ductility, load-carrying capacity, and toughness of concrete [4, 5].

Continuous development in concrete technology has produced ultra-high performance concrete (UHPC) in the 1990s. UHPC represents an advanced generation of cement-based composites consisting of fine and ultra-fine cementitious materials [6]. The coarse aggregate is omitted to approach the homogeneity. The water to cementitious materials ratio (w/cm) is reduced to minimize the porosity and enhance the strength. UHPC depends on optimizing the packing density of the composite [7]. It exhibits outstanding features in compression, tension, and flexural behavior, besides durability, stiffness, and toughness due to using steel fibers [2, 4, 8].

The use of UHPC has significant benefits on the size and the structural behavior of the members [9]. Yoo and Yoon [6] recommended that the very high strength of UHPC could reduce the weight of the structural element by about (⅓ to ½) the element weight of conventional concrete subjected to the same loading.

There have been several studies to determine the bending strength of FRC beams [9, 10, 11, 12, 13, 14, 15]. Oh [11] derived a set of equations for calculating the flexural strength of fibrous reinforced concrete beams. Oh's equations consider the effect of three fiber-related parameters. Fiber orientation, fiber length, and bonding features of fibers were applied to predict the fibrous concrete strength.
Khalil and Tayfur [9] proposed the same set of Oh equations with some moderated and concluded values to predict the flexural strength of UHPC beams. They neglected the matrix tensile strength as Oh assumed and considered the same parameters for fibers adopted by Oh [11]. Rjoub [12] also proposed a set of equations to predict the moment capacity of steel fiber reinforced concrete beams. Yoo et al. [13] adopted micromechanics-sectional analysis to anticipate the flexural strength of UHPC beams. They regarded the pre-cracking and post-cracking tensile behavior of UHPC in the derived equations.

2. The Study's Significance

The available equations for analysis and design of the traditional beams disregard the concrete tensile strength, while UHPC exhibits considerable tensile strength. On the other hand, the very few available methods for the analysis of fibrous concrete underestimate the beam capacity that UHPC beams can withstand. Therefore, there is a need to study the bearing capacity of UHPC beams in flexure.

This study presents a method for predicting the bending moment of reinforced UHPC beams having different types

*E-mail address: adilmahdi@uowasit.edu.iq
ISSN: 1791-2377 © 2022 School of Science, IHU. All rights reserved.
doi:10.25103/jestr.152.13

and volume fractions of fibers. The prime variables that influence the structural behavior of UHPC in compression and tension are adopted to predict the tensile stress, the location of the neutral axis of the beam section, and the bending moment of the UHPC beam. A new factor representing silica fume content, which affects the bonding strength between fibers and the matrix, is adopted to estimate the beam tensile stress. That is because the silica fume content affects the bond force between concrete components on the one hand and between the matrix and the fibers on the other hand. Also, the tensile strength of the matrix is considered and not neglected, as Oh [11] and Khalil and Tayfur [9] assumed, because it provides an initial resistance to forming cracks in the tensile part of the beams, then is followed by resisting bonding between the fibers and the matrix. The study depends on previous experimental work conducted by the author and some studies of other researchers.

3. Behavior of UHPC in Tension and Compression

UHPC exhibits reasonable tensile behavior as the tensile strength is about 4-8 times that of NSC [9]. The fibers dispersed in the matrix provide relatively high confinement, which increases the tensile strength and hinders the emergence and then propagation of cracks. When cracks arise, the fibers bridge them to provide more stiffness. Therefore, pre-cracking and post-cracking tensile stress effectively influence the behavior of beams upon loading [16]. Tensile strength primarily depends on bond strength, which is affected by silica fume content, fibers' content, shape, diameter, and length.

On the other hand, strain hardening and strain softening in compression affect the beam behavior upon loading [16]. The ultra-high-strength increases the compressive area by lowering the depth of the neutral axis from the top of the beam section, which in turn increases its bendability. Therefore, the analysis of the bearing capacity of beams needs analysis of the behavior of the constituted concrete in compression and tension in terms of strength and corresponding strains, besides the area and yield stress of tensile rebars.

4. Flexural Behavior of UHPC Beams Upon Loading

Adding steel fibers to concrete can improve the flexural moment, stiffness, and cracking pattern of reinforced concrete beams, while ductility might be reduced because of crack localization [17]. Several researchers [18, 19, 20, 21] stated that increasing the volume fraction of fibers can inversely affect the flexural ductility of low reinforced beams. Therefore, a high reinforcement ratio is required in UHPC beams to benefit from the ultra-high compressive strength and deflection capacity. Husgul et al. [17] found that an increase of 23-50 % in moment capacity was obtained when using fibers in UHPC compared to the moment of non-fibrous ones. More increment in the moment was obtained in low reinforced beams. When the reinforcement ratio increased, the contribution of the fibers to the beam capacity decreased [17].

Upon loading the reinforced UHPC beam, several micro-cracks develop in the flexural zone. After first cracking, new micro-cracks initiate between the existing ones upon increasing the load. Most cracks propagate toward the upper face, while the pre-cracks do not widen until the stress is concentrated at the critical one to cause the failure [15, 16]. This behavior indicates the ability of fibrous UHPC to redistribute the stresses along the beam sections and withstand high flexural stresses.

The pullout of fibers from the matrix occurs when the load carried by fiber overcomes the bond strength. The stress of failed fiber is transmitted to the neighboring one to bear higher stress and likewise fails when the stress it sustains is greater than the bonding strength. This process continues until all the fibers in the crack region have withdrawn [15, 16].

Many factors affect the tensile strength of UHPC and, to a lesser extent, the compressive strength. Those factors must be considered in the analysis and design of UHPC beams. The factors adopted in this study are as follows;

4.1. Volume fraction of fibers

Increasing fibers' content raises compressive and tensile strength for a limited volume fraction. However, adding steel fibers improves the tensile strength more than the improvement of compressive strength [2, 16].

Lee et al. [22] found that the fiber stress increases in HSC with increasing volume fraction higher than in NSC, which refers to increasing the bonding strength. The stress increment decreases as the fibers' volume fraction increases from 0.5 to 2.0. That means the fiber efficiency decreases as the volume fraction increases.

4.2. Fibers shape

Wille et al. [23] demonstrated that the addition of twisted steel fibers improved post-cracking tensile strength more than short straight fibers in UHPC. That improvement was due to increasing the contact area between the matrix and fiber. The increment ratio can estimate to be 20% [9,24].

4.3. Fibers length and diameter

Yoo et al. [13] stated that the longer the straight steel fibers, the higher the flexural capacity than the shorter ones. Also, the higher the aspect ratio of fibers, the higher flexure, deflection capacity, and absorption energy. These improvements resulted from expanding the effective bonding area between fibers and the contact matrix. It was evident that bonding strength increases with increasing fiber's length and decreasing its diameter.

4.4. Fibers orientation

The orientation and uniform distribution of the fibers through hardened concrete have a significant role in the resulting tensile and flexural strength. When the direction of fibers is perpendicular to the applied load with uniform spacing distribution among them, the tensile strength is higher than that of inclined or irregular distributed fibers [2].

The pouring process and the flowability of UHPC affect the fibers' orientation in the structural elements [15]. For attaining the best results, the flowing of fibrous concrete should be poured into the mold or framework from one side with vibration to maintain a one-direction fibers flow [2, 16].

4.5. Silica fume effect

Chan and Chu [25] experimentally studied the effect of silica fume content on the bond strength and pullout energy of steel fibers in the UHPC matrix. They found that adding silica fume could effectively enhance the bond strength between fibers and the matrix. The optimum silica fume content ranged between 20 -30 % of cement content.

Silica fume contributes to improving the packing density and reducing the relatively large calcium hydroxide crystals in the microstructure of the concrete by reacting with them

[25, 26], providing a high percentage of calcium silicate hydrates (C-S-H), reducing the pore size, and thus increasing bonding strength to the adjacent fibers.

For obtaining the best performance of using silica fume in the mix, the concrete should be heated at (80-90) °C. Heat treatment accelerates the reaction between calcium hydroxide produced on cement hydration and SiO_2 in silica fume to produce more products of C-S-H [2, 27]. Increasing silica fume content raises the modulus of rupture of UHPC. However, the increment range decreases as the silica fume content increase up to 30 % [16, 28].

5. The bond strength between fibers and UHPC Matrix

A mutual transfer of stresses between concrete matrix and fibers is the relation that controls the bearing capacity and stiffness of the UHPC and SFRC beams [29]. The stress transfer relates to the bond force between steel fibers and the contact matrix, which can depict as a frictional force between them.

6. Compressive Behaviour of UHPC in the Beam Section

Based on research findings [2, 3, 14, 16, 30], UHPC exhibits a linear behavior up to approximately 80% of its compressive strength (f'_{cf}). The strain reaches (0.0028-0.0032) at compressive strength and continues to (0.0038-0.0044) at fracture. Fig. 1.a shows the compressive stress-strain relation of UHPC, which can consider for beam-section analysis.

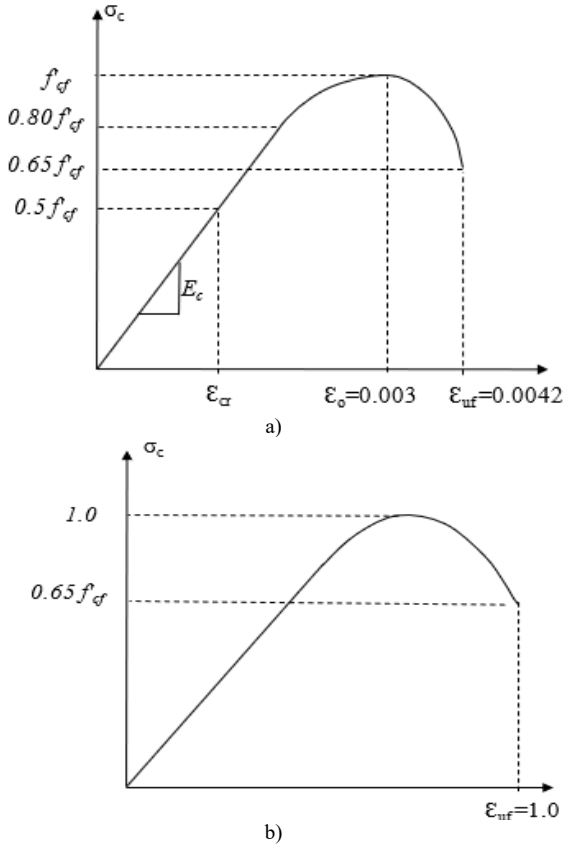

Fig. 1. Stress-strain relationship of UHPC in compression a) Compressive stress – strain of UHPC and b) Compressive stress- strain relation as unit. .

The linear behavior of UHPC to 80% of the compressive strength does not indicate that the cracks started at that stress which means they may have begun before that stress, where the presence of fibers hindered its progress. Therefore, the beginning crack-stress can be adopted at 50% of compressive strength, and the cracking strain can be calculated as follows;

$$\varepsilon_{cr} = \frac{0.5\, f'_{cf}}{E_c} \quad (1)$$

6.1. Equivalent Compressive Stress of UHPC in Sectional Analysis

The compressive force of a rectangular section of UHPC beam is equal to the product of the area under the compressive stress-strain curve by the section width. The resultant force can be computed by the integration method or summation of the finite elements by the trapezoidal technique. For Simplicity, the equivalent stress block of UHPC compressive behavior, which was first time introduced in 1947 by Witney, is adopted in this study. The area of a stress-strain curve can be calculated as shown in Fig. 1.b. The analysis depends on the following data;

$$\varepsilon_{uf}=0.0042 \qquad \varepsilon_o=0.003 \qquad f'_{cf}=151.24\ MPa \quad (2)$$

For estimating the area of the stress-strain curve, the ultimate strain and the compressive strength are assumed to be unity, as illustrated in Fig. 1.b;

$$\varepsilon_{cu}=1.0 \text{ and } f'_{cf}=1.0,$$

Thus, the total area under the compressive stress-strain curve = 0.6235, and the moment of the area about σ_c-axis (neutral axis) = 0.3815

The centroid of the area under curve from σ_c-axis (neutral axis) = 0.612,

And the location of the center from beam top = 1- 0.612 = 0.388 ≈ 0.39

To find the equivalent rectangular area of compression stress: Let length of rectangle equal to twice the centroid distance from σ_c-axis for coinciding the centroid of rectangle with that of the area under the curve.

Hence, the length of the rectangle = 0.388 × 2 = 0.776 ≈ 0.78, which represents the distance from the upper compression fiber of the beam toward the neutral axis position.

Then, the rectangle area = 0.78 c × γ f'_{cf}.

The equivalent compressive strength = 0.8 f'_{cf}, as shown in Fig. 2.

7. Tensile Behavior of UHPC in the Beam Section

Several methods have been improved to predict the tensile strength of steel fiber concrete. Although these methods differ in their approaches, they share the same criteria on which the tensile strength depends. These criteria include fiber orientation, volume fraction, fiber efficiency, and bond strength [22, 31].

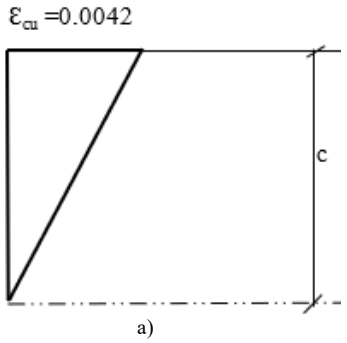

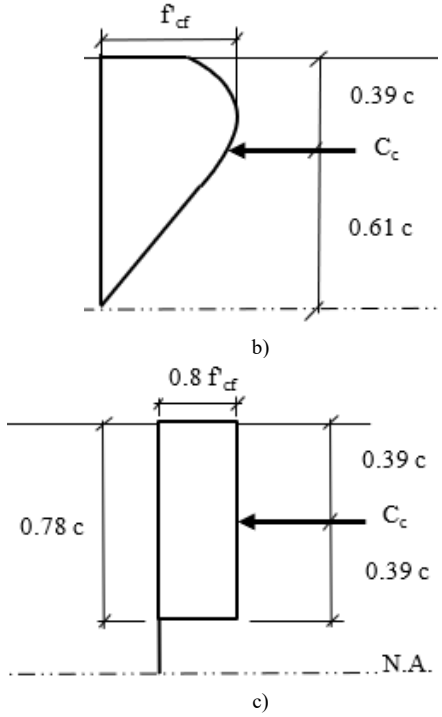

Fig. 2. Compressive strain, stress, and equivalent stress block of UHPC in the beam section a) Compressive strain, b) Real Compressive stress and c) Equivalent compressive stress. .

For simplicity, the adopted tensile stress-strain relationship in this study consists of ascending linear portion up to tensile strength, which represents the elastic behavior of UHPC. The regression portion after peak stress describes the strain-softening until failure by the pullout of all fibers at the crack path. Such behavior can stand for stiffness degradation due to cracking and debonding fibers from the matrix. The strain-softening is assumed to reach 24 times the cracking strain to explain the gradual stiffness loss with the progressive debonding of fibers from the matrix and widening the crack until debonding of the whole fibers at 24 ε_{cr}. The estimated cracking strain (ε_{cr}) for UHPC is between (0.00025-0.0005). The crack strain can be calculated as follows:

$$\varepsilon_{cr} = \frac{f_t}{E_c} \tag{3}$$

Modulus of elasticity is assumed to be the same one calculated from compressive stress-strain relation.

According to the above tensile stress-strain relation, the maximum strain that concrete reached is 0.0048-0.0072, which is consistent with what aforementioned that the strain upon failure approaches 0.01 [32, 33]. Thus, the stress-strain relation of UHPC in compression and tension can visualize in Fig. 3.

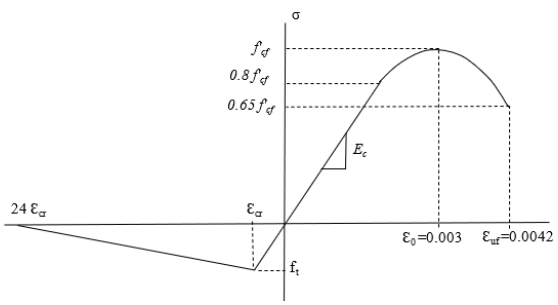

Fig. 3. Stress-strain relationship of UHPC in compression and tension.

7.1. The equivalent Tensile stress of UHPC in Sectional Analysis

To convert the triangular area of tensile stress into an equivalent rectangular one, it must match the centroid of the two areas, as follows;

According to Fig. 4 and from tensile strain diagram;

$$\frac{\varepsilon_{cr}}{24\,\varepsilon_{cr}} = \frac{y_1}{(h-c)} \quad , \qquad y_1 = \frac{(h-c)}{24} \tag{4}$$

From the triangular tensile stress diagram of Fig. 4, the tensile force (F_t) is;

$$F_t = \frac{f_t}{2}\,(h-c) \tag{5}$$

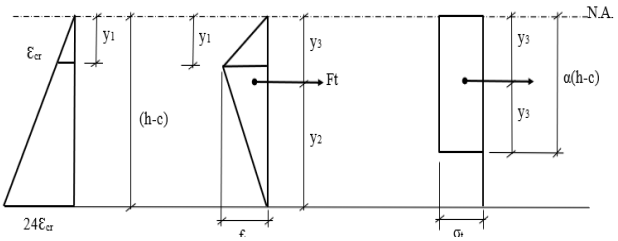

Fig. 4. Tensile strain, stress, and equivalent stress block of UHPC in the beam section.

From the rectangular tensile stress diagram of Fig. 4, the tensile force (F_t) is;

$$F_t = \alpha\,(h-c)\sigma_t \tag{6}$$

By equating equations (5) and (6);

$$\sigma_t = \frac{1}{\alpha}\,\frac{f_t}{2} \tag{7}$$

To find the centroid of the triangular area, the first moment of triangular area is taken around the neutral axis;

$$M_{N.A.} = \frac{f_t}{2}\,y_1\left(\frac{2}{3}\,y_1\right) + \frac{f_t}{2}\,[\,(h-c)-y_1][y_1 + \frac{1}{3}\{(h-c)-y_1\}] \tag{8}$$

Replacing y_1 by $\frac{(h-c)}{24}$;

$$M_{N.A.} = \frac{25\,f_t}{144}\,(h-c)^2 \tag{9}$$

The area of triangle;

$$A = \frac{f_t}{2}(h-c) \tag{10}$$

Thus, the centroid of the triangle area from the neutral axis is;

$$y_3 = \frac{M}{A} = \frac{50}{144}(h-c) \approx 0.35\,(h-c) \tag{11}$$

To coincide the centroid of rectangular area with the triangular one;

$$\alpha\,(h-c) = 2 \times 0.35\,(h-c) = 0.7\,(h-c) \tag{12}$$

The tensile force of rectangular area is;

$$T_{cf} = 0.7\,\sigma_t b\,(h-c) \tag{13}$$

7.2. The bonding strength and tensile stress

Before matrix cracking and at an early stage of loading, the tensile behavior of fibrous matrix can describe as elastic shear at the interface of steel fiber and matrix [34]. That means the bond stress can describe as frictional stress between the concrete matrix and the fiber, as shown in Fig. 5. Therefore, the matrix withstands the tensile stress firstly regarding the confinement effect of steel fibers to increase the tensile stress [16]. After cracking, the steel fibers resist the stress. Therefore, the tensile stress of UHPC depends on matrix tensile strength without fibers and fiber action after crack initiation.

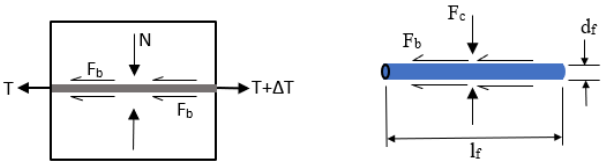

Fig. 5. The friction force between fiber and matrix.

The bond force between concrete matrix and fibers (τ_b) depends on fiber type, length, and diameter, besides the compression force of the surrounding concrete. The bond increases with increasing fiber length and decreasing diameter.

The friction coefficient can be calculated depending on the modulus of rupture of UHPC (f_{rf}), where;

$F_b = \mu F_c$, where F_b is the bonding force, F_c is the UHPC compressive force, and μ is the coefficient of friction between fiber and matrix (14)

$N = F_c$ *(the normal force acting on the area surrounded the fiber)* (15)

$F_b = f_{rf} b\, h$ for prism with cross-section of (b x h), (16)

$F_c = f'_{cf} \times A_{cylinder}$ (17)

$\mu = \frac{f_{rf}\, b\, h}{f'_{cf}\, A_{cyl}}$ *where,* $A_{cyl} = \pi/4\,(D_{cyl})^2$ (18)

An experimental test was conducted on prisms and cylinders [16], as listed in Table 1. The friction coefficient can be calculated according to equation (18).

$F_b = 0.114\, F_c$ (19)

The bond strength for one fiber (τ_b) : $\tau_b = \frac{F_b}{A_{cont}}$, A_{cont} is the surface area along the length of fiber;

$A_{cont} = \pi\, d_f l_f$ (20)

$\tau_b = \frac{0.114\, F_c}{\pi\, d_f l_f}$ (21)

Table 1. Average of coefficient of friction between steel fibers and UHPC matrix.

V_f %	Cylinder compressive strength, MPa	Modulus of rupture(f_{rf}), MPa.	$Fc = f'_{cf} * A_{cyl.}$	$Fr = f_{rf} * b*h$	μ	$\mu_{avg.}$
0.5	112.53	20.00	883.809	98.00	0.111	
1.0	127.00	23.55	997.456	115.40	0.116	0.114
1.5	137.20	25.05	1077.566	122.75	0.114	

7.2.1. The compression force (Fc) subjected on fiber from concrete

Let the compression stress on the fiber is resulted from a square area with length (l_f) over the fiber, in a cube element with length (l_f), as shown in Fig. 6.

$F_c = f'_{cf} * A = f'_{cf} * (l_f)^2$ (22)

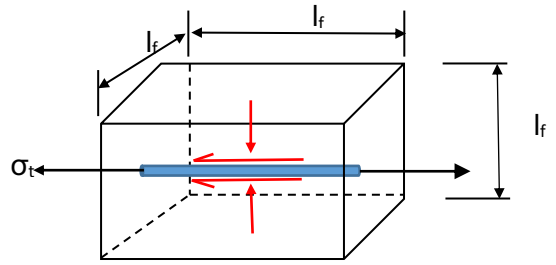

Fig. 6. A cube element to represent the concrete surrounding the fiber.

By considering the quantity of fibers (V_f), the bond strength in the cube element becomes;

$\tau_b = \frac{0.114\, f'_{cf}\,(l_f^2)}{\pi\, d_f l_f} V_f = 0.036\, f'_{cf} \left(\frac{l_f}{d_f}\right) V_f$ (23)

7.2.2. To consider the orientation of fibers

Let half the fibers be oriented by 45 degrees with the horizontal line while the other half is straight.

$\tau_{b\,avg.} = \{ 0.036\, f'_{cf} \left(\frac{l_f}{d_f}\right) cos\, 45 + 0.036\, f'_{cf} \left(\frac{l_f}{d_f}\right) \} V_f / 2$ (24)

$\tau_{b\,avg.} = 0.031\, f'_{cf} \left(\frac{l_f}{d_f}\right) V_f$ (25)

7.2.3. To consider the shape of the fibers

A fiber shape factor (α_b) is used with the above equation, where;

α_b = 1.0 for straight fiber, and

α_b = 1.2 for crimped or hooked ends fiber. The equation of bond strength will be;

$\tau_{b\,avg.} = 0.031\, \alpha_b\, f'_{cf} \left(\frac{l_f}{d_f}\right) V_f$ (26)

7.2.4. To consider the effect of silica fume content

Silica fume content affects the bonding strength between

fibers and the matrix. Therefore, it must be considered in calculating the bonding strength. Hence, the bond strength can be calculated as follows;

$$\tau_{b\,avg.} = 0.031\ \alpha_b\ \beta_{SF}\ f'_{cf}\left(\frac{l_f}{d_f}\right)\ V_f \quad (27)$$

β_{SF} represents the silica fume effect factor on the bond strength of UHPC.

β_{SF} = 1.0 when Silica Fume content ≥ 25% of cement content.
= 0.7 for Silica Fume content = 20% of cement content.
= 0.5 for Silica Fume content ≤15% of cement content.

7.3. The tensile stress

As stated previously, the matrix firstly resists the tensile stress due to the confinement effect of steel fibers. The matrix strength is assumed to be (6.0) MPa depending on the data presented by Khalil and Tayfur [9] for the tensile strength of UHPC without fibers. The tensile stress is calculated as follows;

$$\sigma_t = 2\ \tau_{b\,avg} + 6.0 \quad (28)$$

$$\sigma_t = 0.062\ \alpha_b \beta_{SF}\ f'_{cf}\ \left(\frac{l_f}{d_f}\right) V_f + 6.0 \quad (29)$$

8. Sectional Analysis of Rectangular UHPC Beam

UHPC beams exhibit bearing capacity even after cracking and show tensile strain to a wide range. The ultimate strength method can be used to analyze and design UHPC beams since it depends on the maximum load that can withstand before fracture, i.e., when the concrete compressive and tensile stresses reach the highest values, besides yielding the tensile rebars. Accordingly, some assumptions can be considered for the analysis and design of UHPC beams, as follows;

a) The stresses at failure are non-linear, while the strains are assumed to be linear.
b) The ultimate strain at fracture of UHPC in compression approaches 0.0042.
c) The highest tensile strain at rupture of UHPC reaches 24 Ɛcr.
d) A bilinear relation is considered for the tensile behavior of UHPC.
e) The concrete pouring into the mold or framework is done from one end.

8.1 Flexural Moment Equations

8.1.1. Bending Moment of Singly Reinforced UHPC Rectangular Beam

According to Fig. 7, the equilibrium condition inside the rectangular section gives;

$$C_c = T_s + T_{cf} \quad (30)$$

$$0.8\ f'_{cf}\ (0.78\ c)\ b = A_s\ f_y + 0.7\ \sigma_t\ b\ (h - c) \quad (31)$$

$$0.624\ f'_{cf}\ c\ b + 0.7\ \sigma_t\ c\ b = A_s\ f_y + 0.7\ \sigma_t\ h\ b \quad (32)$$

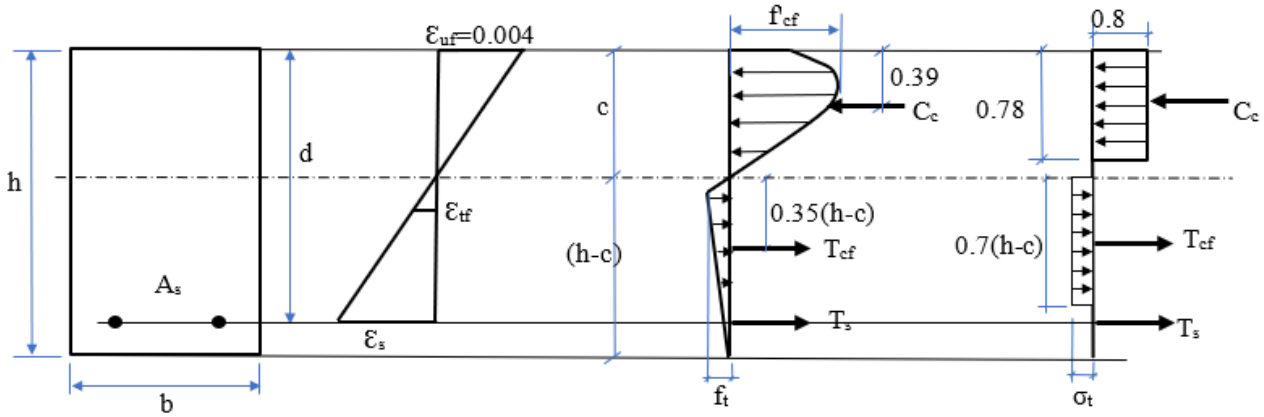

Fig. 7. Singly reinforced UHPC beam cross-section with strains and stresses action.

The distance of neutral axis from the top of section is;

$$c = \frac{A_s\ f_y + 0.7\ \sigma_t\ b\ h}{\left(0.624\ f'_{cf} + 0.7\ \sigma_t\right) b} \quad (33)$$

By taking a moment about the compression force axis, the bending moment is;

$$M_n = T_s(d - 0.39\ c) + T_{cf}\ \{0.35(h - c) + (c - 0.39\ c\ )\} \quad (34)$$

$$M_n = A_s\ f_y\ (d - 0.39c) + 0.7\ \sigma_t\ b\ (h - c)(0.35h + 0.26\ c) \quad (35)$$

8.1.2 Bending Moment for Doubly Reinforced UHPC Rectangular Beam

According to Fig. 8, the equilibrium inside the section;

$$C_c + C_s = T_{cf} + T_s \quad (36)$$

$$0.8\ f'_{cf}\ (0.78c)\ b + A'_s f'_s = A_s f_y + 0.7\ \sigma_t\ b\ (h - c) \quad (37)$$

$$c = \frac{A_s\ f_y - A'_s f'_s + 0.7\ \sigma_t b\ h}{\left(0.624\ f'_{cf} + 0.7\ \sigma_t\right) b} \quad (38)$$

$$M_n = A_s f_y (d - 0.39c) + 0.7\ \sigma_t\ b\ (h - c)(0.35h + 0.26c) + A'_s f'_s (0.39\ c - d') \quad (39)$$

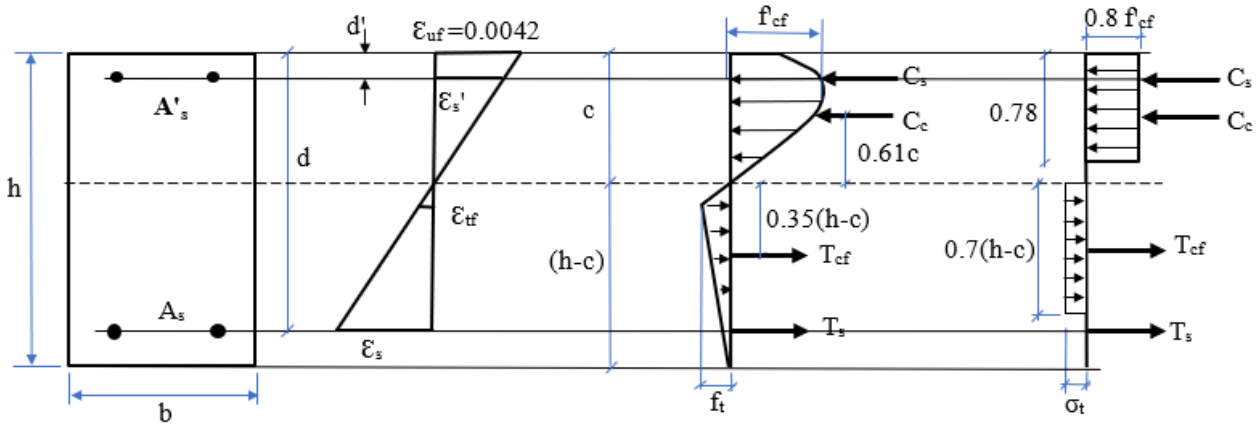

Fig. 8. Doubly reinforced UHPC beam cross-section with strains and stresses action.

For checking the compression rebar whether the yield has arrived or not, strain compatibility is considered;

$$\frac{\varepsilon\prime_s}{0.0042} = \frac{c-d\prime}{c}, \text{ and } \varepsilon'_s = 0.0042\ (\frac{c-d\prime}{c}) \quad (40)$$

$$f'_s = \varepsilon'_s\, E_s, \text{ and } \quad Es = 200000\ MPa \quad (41)$$

$$f'_s = 840\ (\frac{c-d'}{c}) \leq fy \quad (42)$$

9. Verification of the proposed equations with the experimental results

Experimental results of the UHPC beam moments implemented by several researchers were compared with the moment calculated from the proposed equations for verifying, as illustrated in Table 2 for singly reinforced UHPC beams and Table 3 for doubly reinforced UHPC beams. The beams executed by other researchers were rectangular with different dimensions and different height to width (h/b) ratios. The proportions, aspect ratio, and shape of fibers were also variable.

For singly reinforced UHPC beams, it can be seen from Table 2 that there were slight variations between the calculated moments and the experimental ones for different compressive strength (102.9-196.7) MPa and different beam sizes. The variation ranged between (0.88 – 1.12) for regular rectangular beam sections (rectangular beams with h/b greater than 1.0) except for the results computed for Khalil and Tayfur beams. For shallow beams with a depth to width ratio of 0.5, the variation was between (0.98 -1.19). Thus, the equations underestimated the experimental results of the shallow beam with an h/b ratio of 0.5. Therefore, a magnification factor is required for this case, and more data is needed to find such a factor. Fig. 9 compares the experimental to the calculated moments by the proposed equations for singly reinforced UHPC beams.

For the results of the moment of Khalil and Tayfur [9] beams, the equations overestimated the experimental results. The variations may be because the steel reinforcement bars did not reach the yielding stress (f_y =461 MPa) since the research did not include the arrival of rebar yielding.

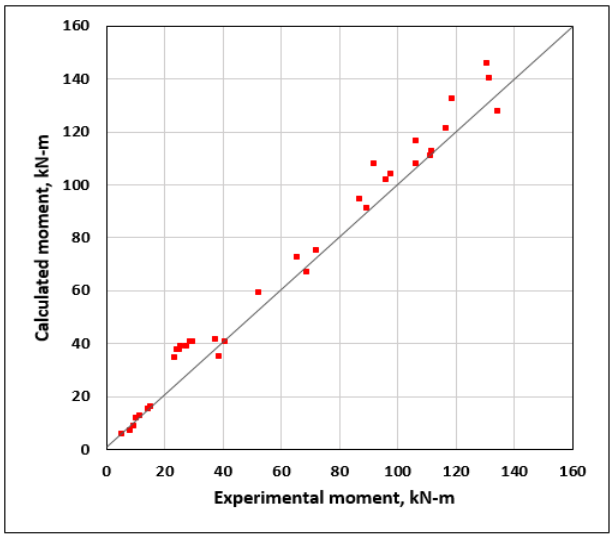

Fig. 9. Comparison of experimental and predicted moments of singly reinforced UHPC beams.

For doubly reinforced UHPC beams, the ratio between experimental to calculated moment ranged between (0.88-1.10). Fig. 10 illustrates the practical and computed moments for doubly reinforced UHPC beams. Generally, the moments resulting from the proposed equations reasonably agree with the experimental results.

It was also noticed that the beams in which concrete was poured from the middle of the mold awarded less bearing capacity than the ones cast from one end and allowed the concrete to flow to the other end to fill the mold, as shown in Table 2 for the third and fourth beams of Yang et al. [15].

According to the compared results in Table 2, the compressive area of the beam section increases with the increase of the tensile reinforcement ratio. That leads to an increase in the bending resistance of the beam when the compressive strength is constant. On the other hand, the increase in the area of tensile reinforcement with increasing compressive strength leads to increasing the compressive region of the beam section. These results are in agreement with the proposed equations.

Table 2. A comparison between calculated moment by the proposed equations to the experimental results of some researches for singly reinforced UHPC beams

Author(s)	A_s mm^2	f_y MPa	f'_{cf} MPa	V_f %	l_f/d_f	b mm	h mm	d mm	P_u kN	a_v m	M_{exp} kN-m	σ_t MPa	c mm	$M_{calc.}$ kN-m	M_{exp}/M_{calc}
Khalil and Tayfur [9]	226	461	137	0	-	150	250	210	79	0.6	23.7	6	19.45	34.53	0.69
	226	461	140	0.5h^{+}	50	150	250	210	84	0.6	25.2	7.302	21.33	37.33	0.68
	226	461	144	0.5c^{++}	50	150	250	210	82	0.6	24.6	7.34	20.83	37.44	0.66
	226	461	141	0.75h	50	150	250	210	92	0.6	27.6	7.97	22.33	38.75	0.71
	226	461	143	0.75c	50	150	250	210	86	0.6	25.8	7.995	22.08	38.82	0.67
	226	461	146	1.0h	50	150	250	210	97	0.6	29.1	8.72	22.84	40.38	0.72
	226	461	149	1.0c	50	150	250	210	100	0.6	30	8.77	22.49	40.52	0.74
Hwan Yang et.al. [15]	0	500	194	2	65	180	270	235	121.7	1.13	68.8	21.64	30.03	66.94	1.03
	253.4	500	194	2	65	180	270	235	154	1.13	87	21.64	35.20	94.40	0.92
	380.1	500	194	2	65	180	270	235	188.6	1.13	106.6	21.64	37.78	107.92	0.99
	380.1	500	194	2	65	180	270	235	163.1	1.13	92.2	21.64	37.78	107.92	0.85*
	506.8	500	194	2	65	180	270	235	206.5	1.13	116.67	21.64	40.36	121.30	0.96
	506.8	500	194	2	65	180	270	215	188.3	1.13	106.4	21.64	40.36	116.23	0.92
	760.2	500	194	2	65	180	270	215	233	1.13	131.65	21.64	45.53	140.06	0.94
Husgul et.al. [17]	301	443	137	0	-	150	250	220	107.13	0.7	37.5	6	21.62	41.61	0.90
	627	462	133	0	-	150	250	218	187.2	0.7	65.52	6	34.19	72.39	0.91
	916	491	135	0	-	150	250	216	275.3	0.7	96.36	6	45.78	101.91	0.95
	1161	468	146	0	-	150	250	200	318.9	0.7	111.62	6	49.03	110.97	1.01
	301	443	157	1.5**	81.25	150	250	220	150.3	0.7	52.61	14.3	31.41	59.10	0.89
	627	463	167	1.5	81.25	150	250	218	256.5	0.7	89.78	14.83	39.54	90.85	0.99
	916	456	157	1.5	81.25	150	250	216	319.73	0.7	111.91	14.3	48.96	112.50	0.99
	1161	465	166	1.5	81.25	150	250	200	383.86	0.7	134.35	14.78	54.29	127.40	1.06
Kamal et.al. [35]	157	500	127	0	65	100	150	117	69.1	0.3	10.365	6	16.96	11.85	0.88
	226	500	127	0	65	100	150	116	98.5	0.3	14.775	6	21.09	15.32	0.97
	157	500	135	0.5	65	100	150	117	78.3	0.3	11.745	7.36	17.43	12.55	0.94
	226	500	135	0.5	65	100	150	116	103.8	0.3	15.57	7.36	21.29	16.02	0.97
Yoo et.al [36]	0	522.7	196.7	2	65	200	270	236	138.1	1.05	72.5	21.85	29.92	75.11	0.97
	253.4	522.7	196.7	2	65	200	270	236	186.5	1.05	97.91	21.85	34.71	103.98	0.94
	506.8	522.7	196.7	2	65	200	270	236	226.2	1.05	118.76	21.85	39.51	132.31	0.90
	760.2	522.7	196.7	2	65	200	270	200	249.5	1.05	130.99	21.85	44.31	145.80	0.90
Pourpapa et.al. [37]	158.8	460	135	1.92	81.25	127	203	180	514.61	0.152	39.11	19.06	33.65	35.09	1.12
	235	460	135	1.92	81.25	127	203	178	538.27	0.152	40.91	19.06	36.48	40.43	1.01
	84.8	460	135	1.92	81.25	152	76	53	73.13	0.152	5.56	19.06	13.02	5.70	0.98
	150.8	460	135	1.92	81.25	152	76	53	110.61	0.152	8.41	19.06	15.07	7.04	1.195
	235	460	135	1.92	81.25	152	76	53	129.12	0.152	9.81	19.06	17.68	8.67	1.13

* the pouring of UHPC was from middle of the mold
$^{+}$h = hooked end fibers were used
$^{++}$c = crimped or twisted fibers were used
** rounded straight fibers were used

Table 3. A comparison between calculated moment by the proposed equations to the experimental results of some researches for doubly reinforced UHPC beams

Author(s)	A_s mm^2	f_y MPa	f'_{cf} MPa	V_f %	l_f/d_f	b mm	h mm	d mm	A_s' mm^2	f_y' MPa	d' mm	P_u kN	a_v m	M_{exp} kN-m	σ_t MPa	c mm	$M_{calc.}$ kN-m	M_{exp}/M_{calc}
Huang et.al. [38]	0	360	102.9	2.0	65	100	200	185	101	300	15	40	0.533	12.00	14.294	26.96	13.33	0.90
	227	360	102.9	2.0	65	100	200	184	101	300	16	102	0.533	27.20	14.294	33.89	26.97	1.01
	509	360	102.9	2.0	65	100	200	182	101	300	19	168	0.533	44.80	14.294	47.57	42.50	1.05
	1018	360	102.9	2.0	65	100	200	172	101	300	28	257	0.533	68.53	14.294	72.26	64.06	1.07
	1256	360	102.9	2.0	65	100	200	170	101	300	30	261	0.533	69.60	14.294	83.81	72.84	0.96
	1520	360	102.9	2.0	65	100	200	168	101	300	32	281	0.533	74.93	14.294	96.61	81.32	0.92
Feng et.al. [24]	1140	494.0	125.4	2h	80	150	300	240	226.2	481.4	50	326	0.95	154.85	20.928	69.87	176.39	0.88
	1742	495.5	125.4	2h	80	150	300	240	226.2	481.4	50	477	0.95	226.58	20.928	88.69	228.89	0.99
	2463	499.3	125.4	2h	80	150	300	240	226.2	481.4	50	662	0.95	314.45	20.928	111.70	287.04	1.10
	1140	494.0	128.4	3h	80	150	300	240	226.2	481.4	50	368	0.95	170.05	28.927	78.00	196.83	0.89
	1742	495.5	128.4	3h	80	150	300	240	226.2	481.4	50	485	0.95	230.38	28.927	95.13	248.17	0.93
	2463	499.3	128.4	3h	80	150	300	240	226.2	481.4	50	636	0.95	302.10	28.927	116.07	305.19	0.99

Increasing silica fume content raises the bonding strength between fibers and the matrix, which, in turn, raises the tensile strength. Also, enriching fibers' content raises the tensile stress, as shown in Table 4.

Upon using the proposed equations to calculate the moment in steel fiber's high strength concrete (HSC) beams, these equations exhibited good agreement with the experimental results, as illustrated in Table 4. A small change was made in the tensile stress equation, assuming the matrix tensile strength to be 3.0 instead of 6.0, as follows;

$$\sigma_t = 0.062\,\alpha_b\beta_{SF}\left(\frac{l_f}{d_f}\right)V_f + 3.0 \tag{43}$$

The variation of experimental to calculated moment ranges between (0.93-1.07) for HSC beams, as shown in Fig. 11.

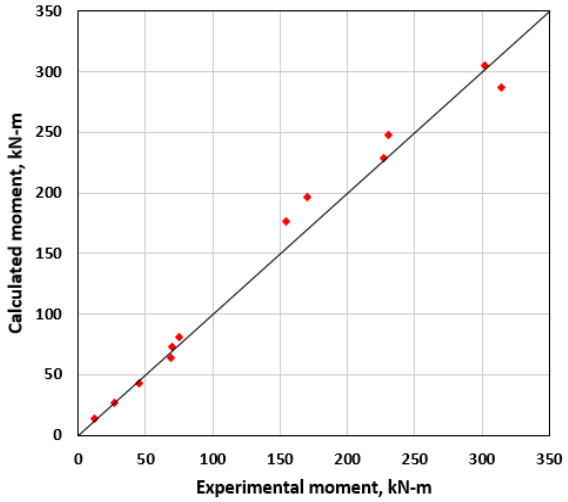

Fig. 10. Comparison of experimental and predicted moments of doubly reinforced UHPC beams.

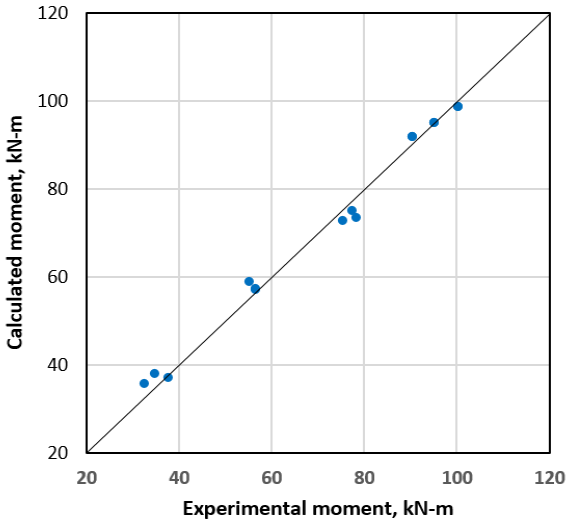

Fig. 11. Comparison of experimental and predicted moments of HSC beams.

Table 4. A comparison between calculated moment by the proposed equations to the experimental results of some researches for singly reinforced HSC beams.

Author(s)	A_s mm²	f_y MPa	f'_{cf} MPa	V_f %	l_f/d_f	b mm	h mm	d mm	P_u kN	a_v m	M_{exp} kN-m	σ_t MPa	c mm	$M_{calc.}$ kN-m	M_{exp}/M_{calc}
Vijayanand et al. [39]	265.8	569	59.12	0	60	125	250	217	94	0.7	32.9	3	44.50	35.54	0.93
	477.5	569	61.11	0	60	125	250	216	162	0.7	56.7	3	67.07	56.62	1.00
	671.4	569	59.12	0	60	125	250	214	216	0.7	75.6	3	91.85	72.69	1.04
	265.8	569	62	0.5c++	60	125	250	217	108	0.7	37.8	3.69	44.96	36.73	1.03
	477.5	569	57.12	0.5c++	60	125	250	216	162	0.7	56.7	3.69	73.75	56.94	0.99
	671.4	569	57.8	0.5c++	60	125	250	214	224	0.7	78.4	3.69	95.78	73.08	1.07
	265.8	569	61.34	1.0++	60	125	250	217	100	0.7	35	4.37	47.77	37.73	0.93
	477.5	569	63.8	1.0++	60	125	250	216	158	0.7	55.3	4.37	68.54	58.73	0.94
	671.4	569	61.8	1.0++	60	125	250	214	222	0.7	77.7	4.37	91.80	74.81	1.04
Ashur 1997 [19]	628	437	87.11	0.5	75	170	300	265	-	-	90.69	7.01	52.09	91.68	0.989
	628	437	88.11	1.0	75	170	300	265	-	-	95.41	8.05	54.52	94.91	1.005
	628	437	90.53	1.5	75	170	300	265	-	-	100.4	9.16	56.24	98.48	1.019
	628	437	87.11	0.5	75	170	300	265	-	-	90.69	7.01	52.09	91.68	0.989
	628	437	88.11	1.0	75	170	300	265	-	-	95.41	8.05	54.52	94.91	1.005
	628	437	90.5	1.5	75	170	300	265	-	-	100.4	9.16	56.25	98.48	1.020

c++ crimped steel fiber

The proposed equations can be used even for beams without reinforcement since the equations gave good agreement with the experimental results.

The differences in results can be due to several reasons, among them;

a) The equations depended on the compressive strength of small control specimens, while for large beams, the resistance might differ because large models are non-controlled.

b) The difference in the theoretical (d) and (d') compared to the practical values may cause the differences. That can result from the movement of the rebar during the casting work.

c) The non-uniform distribution of fibers within the beam and the possibility of its concentration in a specific location and leaving other sites to have no fiber or have fewer fibers may cause those differences.

d) The difference in the method of pouring and the direction of the concrete in the mold causes the differences.

10. Conclusions

This paper presents a theoretical study to analyze UHPC beams in flexure. The analysis regards several factors that influence the behavior of UHPC beams upon loading to cause flexural failure. The following conclusions can derive;

1. Increasing the tensile strength and enhancing the ductility of UHPC beams can minimize the ratio of steel reinforcement. However, a high reinforcement ratio is required in UHPC beams to benefit from ultra-high compressive strength and deflection capacity.
2. The fibers dispersed in the UHPC matrix provide relatively high confinement to delay the cracking of the matrix. After cracking, the fibers bridge the two sides of the crack to provide high ductility, and the tensile strength increases more. Therefore, the fibers have dual action to enhance tensile strength. That means the tensile stress consists of matrix strength and fiber contribution in bearing stress.
3. The tensile strength of fibrous UHPC relies on several factors. Some of them were previously considered by other researchers as volume fraction, shape, aspect ratio, and orientation of fibers. A new factor considered in this study is the effect of silica fume content on the bonding strength

between steel fibers and the contact matrix.

4. A bilinear elastic-strain softening model for simulation of tensile strength of UHPC is considered in predicting the sectional tensile stress. The ultimate strain reaches 24 times cracking one.
5. Several equations are proposed to predict the flexural moment of UHPC, the location of the neutral axis, and the tensile stress of UHPC in the rectangular beam section with single or double reinforcement.
6. The proposed equations award a good agreement with the experimental results for singly and doubly reinforced UHPC beams and for HSC.

This is an Open Access article distributed under the terms of the Creative Commons Attribution License.

References

1. Azmee, N. M. and Shafiq, N. (2018) 'Ultra-high performance concrete: From fundamental to applications', *Case Studies in Construction Materials*, 9(September), p. e00197. doi: 10.1016/j.cscm. 2018.e00197.
2. Fehling, E.; Schmidt, M.; Walraven, J.; Leutbecher, T.; Frohlich, S.; (2014), "*Ultra-High Performance Concrete, Fundamentals, Design, Examples*", Beton Kalender, Wilhen Ernst and Sohn, Germany, 188p.
3. Benjamin A., G. (2006) 'Material Property Characterization of Ultra-High Performance Concrete', *Fhwa, (FHWA-HRT-06-103),* p. 186.
4. Jabbar, A. M., Hamood, M. J. and Mohammed, D. H. (2021) 'Ultra-High Performance Concrete Preparation Technologies and Factors Affecting the Mechanical Properties: A Review'*, IOP Conference Series: Materials Science and Engineering*, 1058(1), p. 012029. doi: 10.1088/1757-899x/1058/1/012029.
5. ACI 239R, "Ultra-high-performance concrete: An emerging technology report," *Am. Concr. Inst*. ACI 239, 2018.
6. Yoo, D. Y. and Yoon, Y. S. (2016) 'A Review on Structural Behavior, Design, and Application of Ultra-High-Performance Fiber-Reinforced Concrete', *International Journal of Concrete Structures and Materials*, 10(2), pp. 125–142. doi: 10.1007/s40069-016-0143-x.
7. de Larrard, F. and Sedran, T. (1994) 'Optimization of ultra-high-performance concrete by the use of a packing model', *Cement and Concrete Research*, 24(6), pp. 997–1009. doi: 10.1016/0008-8846(94)90022-1.
8. Hung, C.-C., El-Tawil, S. and Chao, S.-H. (2021) 'A Review of Developments and Challenges for UHPC in Structural Engineering: Behavior, Analysis, and Design', *Journal of Structural Engineering*, 147(9), p. 03121001. doi: 10.1061/(asce)st.1943-541x.0003073.
9. Khalil, W. I. and Tayfur, Y. R. (2013) 'Flexural strength of fibrous ultra-high performance reinforced concrete beams', *ARPN Journal of Engineering and Applied Sciences*, 8(3), pp. 200–214.
10. ACI Committee 544, "Design Consideration for Steel Fiber Reinforced Concrete", *ACI 544.4R-88*, reapproved 1999, 18 pp.
11. B.H. Oh, (1993) "Flexural Analysis of Reinforced Concrete Beams Containing Steel Fibers", *Journal of Structural Engineering*, Vol. 118, Issue 10, ASCE, p.2821-2835.
12. M.I.M. Rjoub, (2006) "Moment Capacity of Steel Fiber Reinforced Concrete Beams", *Journal of Engineering Sciences, Assiut University*, Vol. 34, No. 2, p.413-422.
13. Yoo, D. Y., Banthia, N. and Yoon, Y. S. (2016) 'Predicting the flexural behavior of ultra-high-performance fiber-reinforced concrete', *Cement and Concrete Composites,* 74, pp. 71–87. doi: 10.1016/j.cemconcomp.2016.09.005.
14. Graybeal, B. A. (2008) 'Flexural Behavior of an Ultrahigh-Performance Concrete I-Girder', *Journal of Bridge Engineering*, 13(6), pp. 602–610. doi: 10.1061/(asce)1084-0702(2008)13:6(602).
15. Yang, I. H., Joh, C. and Kim, B. S. (2011) 'Flexural strength of ultra-high strength concrete beams reinforced with steel fibers', *Procedia Engineering*, 14, pp. 793–796. doi: 10.1016/j.proeng.2011.07.100.
16. Jabbar, A. M., Hamood, M. J. and Mohammed, D. H. (2021) 'The effect of using basalt fibers compared to steel fibers on the shear behavior of ultra-high performance concrete T-beam', *Case Studies in Construction Materials*, 15, p. e00702. doi: 10.1016/j.cscm. 2021.e00702.
17. Hasgul, U. et al. (2018) 'Flexural behavior of ultra-high-performance fiber reinforced concrete beams with low and high reinforcement ratios', *Structural Concrete*, 19(6), pp. 1577–1590. doi: 10.1002/suco.201700089.
18. Yoo, D. Y. and Yoon, Y. S. (2015) 'Structural performance of ultra-high-performance concrete beams with different steel fibers', *Engineering Structures,* 102, pp. 409–423. doi: 10.1016/j.engstruct.2015.08.029.
19. Beshara, F. B. A., Shaaban, I. G. and Mustafa, T. S. (2012) 'Nominal Flexural Strength of High Strength Fiber Reinforced Concrete Beams', *Arabian Journal for Science and Engineering,* 37(2), pp. 291–301. doi: 10.1007/s13369-012-0172-y.
20. Dancygier AN, Savir Z. Flexural behavior of HSFRC with low reinforcement ratios. *Eng Struct*. 2006; 28:1503-1512. https://doi.org/10.1016/j. engstruct.2006.02.005
21. Yoo DY, Banthia N, Yoon YS. Experimental and numerical study on flexural behavior of UHPFRC beams with low reinforcement ratios. *Can J Civ Eng.* 2017;44(1):18-28. https://doi.org/10.1139/cjce-2015-0384.
22. Lee, S. C., Oh, J. H. and Cho, J. Y. (2016) 'Fiber efficiency in SFRC members subjected to uniaxial tension', *Construction and Building Materials*, 113, pp. 479–487. doi: 10.1016/j.conbuildmat.2016.03.076.
23. Wille K, Kim DJ, Naaman AE. Strain-hardening UHP-FRC with low fiber contents. *Mater Struct* 2011;44(3):583–598.
24. Feng, Z. et al. (2021) 'Flexural and cracking behaviors of reinforced UHPC beams with various reinforcement ratios and fiber contents', *Engineering Structures,* 248 (December). doi: 10.1016/j.engstruct.2021.113266.
25. Chan, Y. W. and Chu, S. H. (2004) 'Effect of silica fume on steel fiber bond characteristics in reactive powder concrete', *Cement and Concrete Research*, 34(7), pp. 1167–1172. doi: 10.1016/j.cemconres.2003.12.023.
26. P., J. Jun, K. S. Tae, K., K. Taek, K., S. Wook, "Influence of the Ingredients on Compressive Strength of Ultra-High Performance Concrete as Fundamental Study to Optimize the Mixing Proportion", *Second International Symposium on Ultra-High Performance Concrete,* Kassel, Germany, March 05-07, 2008, p.105-112.
27. Alsalman, C. N. Dang, J. R. Martí-Vargas, and W. Micah Hale, "Mixture-proportioning of economical UHPC mixtures," *J. Build. Eng*., vol. 27, (February 2019), 2020, doi: 10.1016/j.jobe.2019.100970.
28. M. M. S. Ridha, K. F. Sarsam, and I. A. S. Al-Shaarbaf, "Experimental Study and Shear Strength Prediction for Reactive Powder Concrete Beams," *Case Stud. Constr. Mater.*, vol. 8, no. March, pp. 434–446, 2018, doi: 10.1016/j.cscm.2018.03.002.
29. Bilek, V. et al. (2017) 'Bond Strength between Reinforcing Steel and Different Types of Concrete', *Procedia Engineering*, 190, pp. 243–247. doi: 10.1016/j.proeng.2017.05.333.
30. P. Máca, R. Sovják, and T. Vavřiník, "Experimental investigation of mechanical properties of UHPFRC," *Procedia Eng*., vol. 65, pp. 14–19, 2013, doi: 10.1016/j.proeng.2013.09.004.
31. P. Marti, T. Pfyl, V. Sigrist, T. Ulaga, Harmonized test procedures for steel fiber-reinforced concrete, *ACI Mat. J*. 99, 1999-676-686.
32. P. Richard and M. Cheyrezy, "Composition of reactive powder concretes," *Cem. Concr. Res*., vol. 25, no. 7, pp. 1501–1511, 1995, doi: 10.1016/0008-8846(95)00144-2.
33. M.M. Reda, N.G. Shrive, J.E. Gillott, Microstructural investigation of innovative UHPC, *Cem. Concr. Res*. 29 (1999) 323 – 329.
34. Kang, S. T. and Kim, J. K. (2012) 'Investigation on the flexural Behavior of UHPCC considering the effect of fiber orientation distribution', *Construction and Building Materials,* 28(1), pp. 57–65. doi: 10.1016/j.conbuildmat.2011.07.003.

35. Kamal, M. M. et al. (2014) 'Behavior and strength of beams cast with ultra-high strength concrete containing different types of fibers', *HBRC Journal*, 10(1), pp. 55–63. doi: 10.1016/j.hbrcj.2013.09.008.
36. Yoo, D. Y., Banthia, N. and Yoon, Y. S. (2017) 'Experimental and numerical study on flexural behavior of ultra-high-performance fiber-reinforced concrete beams with low reinforcement ratios', *Canadian Journal of Civil Engineering*, 44(1), pp. 18–28. doi: 10.1139/cjce-2015-0384.
37. Pourbaba, M., Sadaghian, H. and Mirmiran, A. (2019) 'A comparative study of flexural and shear behavior of ultra-high-performance fiber-reinforced concrete beams', *Advances in Structural Engineering*, 22(7), pp. 1727–1738. doi: 10.1177/1369433218823848.
38. Huang, J. et al. (2021) 'Flexural behavior and evaluation of ultra-high-performance fiber reinforced concrete beams cured at room temperature', *Scientific Reports*, 11(1), pp. 1–16. doi: 10.1038/s41598-021-98502-x.
39. Vijayanand, M. Et Al. (2010) 'Flexural Characteristics of Steel Fiber Reinforced Self Compacting Concrete Beams', The Scientific Bulletin of Valahia University –*Materials and Mechanics*, 5(5), pp. 1–7.

Nomenclature

As	*Tensile steel reinforcement area, mm²*
As'	*Compressive steel reinforcement area, mm²*
a_v	*Shear span, mm*
b	*Width of beam cross-section, mm*
c	*Distance of neutral axis from top of the beam section, mm*
Cc	*UHPC compression force, N*
Cs	*Steel rebar compressive force, N*
d	*Effective depth of beam cross-section, mm*
d'	*Distance from top of the beam section to the centre of compression rebars, mm*
df	*Fiber diameter, mm*
Ec	*Elastic modulus of UHPC, MPa*
$\mathcal{E}_{cr}$	*Cracking strain of UHPC in tension or compression*
$\mathcal{E}_o$	*Strain of UHPC at f'cf in compression*
$\mathcal{E}_{uf}$	*Ultimate strain of UHPC in compression*
F_b	*Friction force between steel fiber and contact matrix, N*
f'_{cf}	*Cylinder compressive strength of UHPC, MPa*
ft	*Maximum tensile strength of UHPC, MPa*
fy	*Yield stress of tensile rebar, MPa*
fy'	*Yield stress of compression rebar, MPa*
h	*Height of beam cross-section, mm*
lf	*Fiber length, mm*
$N=Fc$	*Normal compressive force of UHPC surrounded the fiber in the cube element, N*
T	*Tensile force subjected on fiber, N*
Tcf	*UHPC tensile force, N*
Ts	*Steel rebar tensile force, N*
V_f	*Volume fraction of steel fiber*
α_o, α_l, α_b	*Fiber orientation, fiber length, and bonding factors*
β_{SF}	*Silica fume affect factor on the bond strength*
μ	*Friction coefficient between steel fiber and contact matrix, N*
σ_t	*Tensile stress of UHPC, MPa*
τ_b	*Bond strength between fiber and contact matrix, MPa*
$\tau_{b\ avg.}$	*Average bond strength between fiber and contact matrix, MPa*